Automated probe microscopy via evolutionary optimization at the atomic scale

Richard A. J. Woolley, Julian Stirling, Adrian Radocea, Natalio Krasnogor, and Philip Moriarty
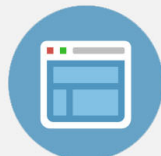
Automated probe microscopy via evolutionary optimization at the atomic scale

Richard A. J. Woolley,[1,a)] Julian Stirling,[1] Adrian Radocea,[2] Natalio Krasnogor,[3] and Philip Moriarty[1]

[1]*School of Physics and Astronomy, University of Nottingham, Nottingham NG7 2RD, United Kingdom*
[2]*Department of Materials Science and Engineering, Cornell University, Ithaca, New York 14853, USA*
[3]*School of Computer Sciences, University of Nottingham, Nottingham NG8 1BB, United Kingdom*

We describe the development and application of an imaging protocol, which evolves a scanning probe's atomic structure in parallel with automated optimization of the scan parameters. Our protocol coerces the system into a state that produces a specific atomic resolution image type without human involvement. © *2011 American Institute of Physics.* [doi:10.1063/1.3600662]

The automation of experimentation has now progressed to the point whereby robot scientists are capable of not only testing hypotheses but, remarkably, of developing the appropriate scientific hypothesis in the first place.[1] Sophisticated experimental optimization based on evolutionary strategies has been demonstrated for a broad range of processes including laser pulse shaping,[2] control of oscillatory chemical systems,[3] the study of Bose–Einstein condensates,[4] and the scheduling of experiments by a robot scientist.[5] Although evolutionary algorithms[6] have been applied to a number of problems in computational nanoscience,[7,8] these algorithmic strategies have hitherto not been incorporated into what is arguably the most important tool for experimentation at the nanoscale: the scanning probe microscope.

Despite recent impressive advances in scanning probe microscopy (SPM) control at the atomic and molecular levels,[9–12] there remains a central component of the probe microscope, which not only produces a significant bottleneck in data collection but, in the vast majority of cases, leads to an inherent uncertainty in the image formation mechanism. The component in question is, of course, the probe itself. Probe microscopists adopt a mixture of experience and serendipity when selecting control parameters that produce tips capable of atomic/molecular resolution. During the optimization of tip and imaging parameters the perceived quality of the image (or line profiles) *is entirely based on operator experience* rather than arising from a well-defined metric (or set of metrics).

To address this issue we have developed a machine learning protocol for the control and optimization of the structure of a scanning probe used for atomic resolution imaging. We demonstrate how the precise state of the probe and the associated control parameters can be automatically tuned by the algorithm so as to provide a particular image type. High quality atomic resolution images are obtained with no human operator involvement other than installation of the tip and sample in the microscope at the start of the experiment.

To assess the ability of the system to evolve high quality images we chose a prototypical tip-sample combination; a PtIr probe scanning a highly oriented pyrolytic graphite (HOPG) sample. The surface was prepared by cleaving with Scotch tape while the 250 μm diameter PtIr wire tip was

simply cut. All scans were carried out in ambient conditions on a simple entry-level scanning tunnel microscope (STM) (EasyScan, Nanosurf). Variation in experimental air temperature was restricted.

The graphite surface is widely used as a standard test for the atomic resolution capabilities of an STM. Despite being studied for decades, however, there remain some open questions regarding the nature of STM images of the HOPG surface and the process by which those images are obtained.[13] As such, the ability to evolve the control parameters and tip state to give rise to different symmetries of the graphite lattice, i.e., trigonal versus honeycomb, was an important objective of the evolutionary strategy we adopted.

Before fine tuning the control parameters, the probe is conditioned at a relatively coarse level, Fig. 1. This initial stage of the optimization process is entirely deterministic and subject to simple rules and image analysis metrics. Initially, a
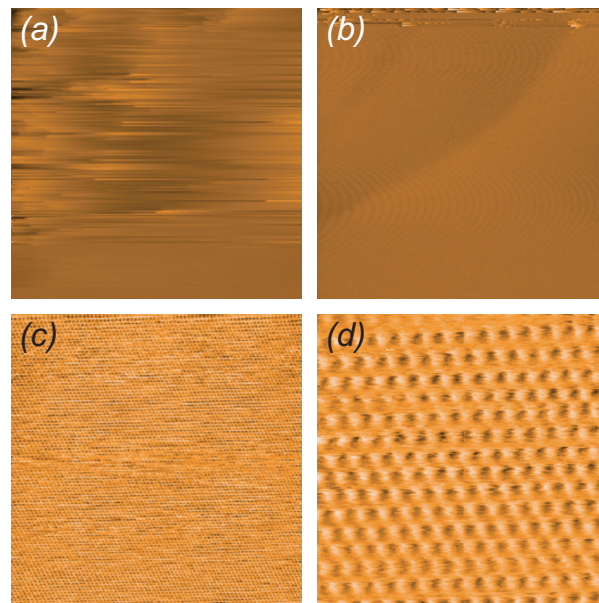

FIG. 1. (Color online) Selection from a sequence of images (slow scan direction from top to bottom) of the graphite (HOPG) surface acquired in the initial "deterministic" phase. Tunnel current=3 nA, sample bias 50 mV, scan rate 0.1 lines/s, 256×256 pixels. After improving the 200 ×200 nm^2 image by applying a 5 V, 200 ms voltage pulse (off the image area), [(a)–(b)], the algorithm zooms in to (c) 20×20 nm^2 and (d) 4 ×4 nm^2.

a)Electronic mail: richard.woolley@nottingham.ac.uk.

large area $(200 \times 200$ nm^2) scan is taken and, following plane removal, the apparent surface morphology is algorithmically ascertained. Poor images are identified by a high surface roughness, and are classified according to their appearance using the universal similarity metric (USM).[14]

At the end of a poor scan (and dependent on image class), voltage pulse(s) are applied and the scan repeated until the image of the surface becomes atomically flat. If this is unsuccessful following a number of attempts, the X-Y scan coordinates are altered to move to a different sample area. Relatively few of the probes, 9%, fail to get past this first stage. We are confident that this figure can be improved upon with other substrate/tip combinations and with operation under vacuum conditions.

After a flat 200×200 nm^2 image is achieved, the system incrementally decreases the scan window size. At each step, the image quality is assessed using a combination of metrics. For scan sizes ≥ 50 nm, the presence of step edges and surface defects are used to ascertain surface quality. If at any stage during this "deterministic" phase the acquired image fails to meet the assessment criteria, different probe-forming routines are employed (e.g., voltage pulsing or high tunnel current imaging). If the surface is measured as atomically flat, the scan size is reduced further, to 20×20 nm^2. At this level, if Fourier analysis reveals structure consistent with the graphite lattice the scan size is reduced to the final magnification level of 4×4 nm^2. Here again the Fourier components are ascertained and, as a quantifiable measure of quality, the scan is cross-correlated with a target image. Once the correlation value passes a certain predetermined threshold evolutionary optimization is initiated.

Our evolutionary optimization algorithm, based on a cellular genetic algorithm (cGA),[15] belongs to a subclass of GAs in which the individual (potential solution) only inherits characteristics from its closest neighbors during the breeding cycle.[16,17] These overlapped small neighborhoods cause a slow diffusion of solutions through the population, enhancing diversity, and exploration while intensification through genetic operations, takes place inside the neighborhood (concentrating genotypes that create fitter individuals). This type of structured algorithm is especially well-suited for complex problems.[18] Here we allow the cGA to evolve the imaging parameters in order to achieve a best match to a target image. Initially, the first generation is seeded with random values from the available parameter space (determined from the physical limits of the system) and assigned to individuals within the population. A generation can consist of any number, n, of individuals (typically 25), I_n, each having a particular set of parameters (genotype), $I_n(i, V, G_I, G_P)$, where i, V, G_I, and G_P are the tunnel current setpoint, the sample bias voltage, integral gain, and proportional gain, respectively. At the end of the generation, when all the images have been acquired, each individual image, I, is compared against the chosen target image and assigned a fitness according to similarity. To aid flexibility the target image is simply input as a scaled bitmap of the required surface. These "ideal" surfaces can be from previous cGA runs, from those produced by the human operator, theoretical representations, or even correctly scaled images from the literature can be used.

The similarity between target and acquired image for the cGA phase is assessed by calculating the robust mutual information (RMI)[19] shared between the two images, rather
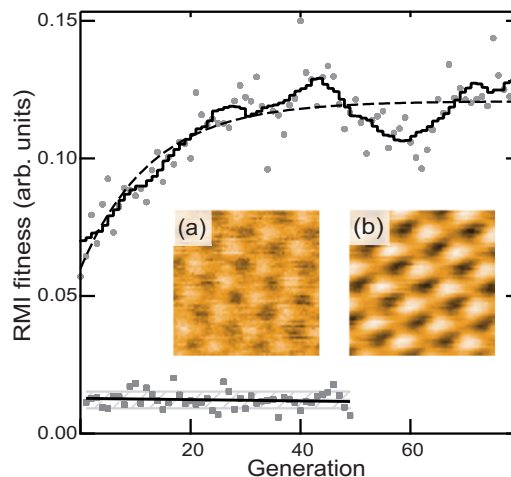

FIG. 2. (Color online) The average evolution of cGA image quality as a function of generation. Closed circles show the averaged fitness values, where the solid line is a Savitzky–Golay smoothing of the data to highlight the evolution. The trend for increase in fitness is highlighted by a dashed line (an exponential fit to the data points) that in this case plateaus at an RMI of 0.12. For comparison, the square markers show the lack of change in fitness for randomly selected imaging parameters (shaded area ± 1 standard deviation). Inset: 1×1 nm^2 (a) the starting image and (b) the evolved image.

than via the USM because of the increased efficiency of the RMI in distinguishing between regular patterns. The higher the RMI value, the fitter the individual. As the population's average fitness increases the mutation rate is slowed—just as a human operator would reduce the variance in the parameter space—as the ideal image is honed in on. Figure 2 shows the evolution of the system toward a higher quality image as a function of the number of cGA generations.

Crucially, the system has the ability to self-tune and evolve to different STM images of the same surface. The selection of a specific image type has particular potential with regard to elucidating (and exploiting) the contribution of the probe structure in SPM imaging, enabling, in principle, "auto recovery" of a given tip state. Figure 3 shows examples of the two primary image types observed for STM imaging of the HOPG surface—the trigonal and honeycomb lattices. These images were acquired by the system evolving and optimizing to different predefined targets [Figs. 3(c) and 3(d)] of the expected surface. A key observation is that it is not just the selection of the parameters themselves that result in a good image. Instead, both the optimized parameters *and*
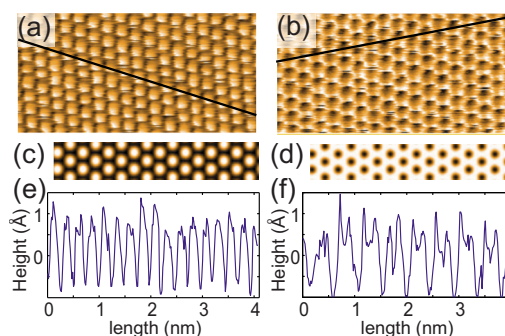

FIG. 3. (Color online) Genetic algorithm-optimized 4×2 nm^2 atomic resolution images showing (a) trigonal and (b) honeycomb symmetry for the graphite surface. The system has tuned itself to the predefined targets shown in (c) and (d), respectively. Line profiles (e) and (f) show the characteristic repeat pattern of carbon atoms for each type of image.
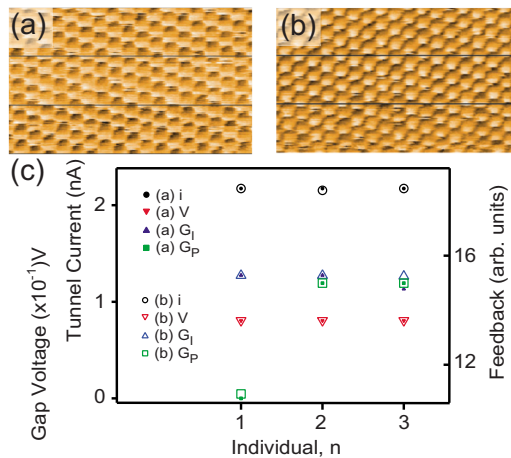
FIG. 4. (Color online) Different images of the same scanned area during the cGA phase [(a) and (b)]. The three individuals (1–3) in each image (delimited by solid black lines) have close to identical imaging parameters, (c).

the history of image optimization, i.e., the path taken in tuning the instrument, are key. Figures 4(a) and 4(b) show that two different surface structures can be obtained with almost identical imaging parameters, Fig. 4(c). This clearly demonstrates the importance of the tip's history and the apparent phenotypic "plasticity," an area we are currently studying.

Scanning probe imaging of graphite has very recently received renewed interest[13,20] due, in part, to the obvious relationship between the ability to understand and measure the HOPG surface and that of graphene. Although an elucidation of the image formation mechanism is outside the scope of this letter, the ability of the automated system we have developed to self-tune to a particular image "class" has obvious potential in the analysis and interpretation of the role of the tip in STM image generation.

The evolutionary protocol we outline here not only coerces an STM to produce high quality atomic resolution images of a particular type but, because any scanning probe image involves a convolution of tip and surface structure, opens up the possibility of intelligently engineering the atomic architecture of the apex of the probe. We expect that evolutionary optimization of scanning probes will find application in both STM and, significantly, qPlus atomic force microscopy[9,11] (where there is much broader parameter

space). There is immense scope for the extension of the cGA approach to more sophisticated machine learning methods, which can handle not only known surface structures but those of unknown symmetry and periodicity.

[1] R. D. King, J. Rowland, S. G. Oliver, M. Young, W. Aubrey, E. Byrne, M. Liakata, M. Markham, P. Pir, L. N. Soldatova, A. Sparkes, K. E. Whelan, and A. Clare, Science **324**, 85 (2009).

[2] D. Zeidler, S. Frey, K. L. Kompa, and M. Motzkus, Phys. Rev. A **64**, 023420 (2001).

[3] R. Toth, C. Stone, A. Adamatzky, B. de Lacy Costello, and L. Bull, J. Chem. Phys. **129**, 184708 (2008).

[4] W. Rohringer, R. Bucker, S. Manz, T. Betz, C. Koller, M. Gobel, A. Perrin, J. Schmiedmayer, and T. Schumm, Appl. Phys. Lett. **93**, 264101 (2008).

[5] E. L. Byrne, *Proceedings of the 2007 GECCO Conference Companion on Genetic and Evolutionary Computation* (ACM, New York, NY, 2007).

[6] J. H. Holland, *Adaptation in Natural and Artificial Systems* (The University of Michigan Press, Ann Arbor, MI, 1975).

[7] N. Dugan and S. Erkoc, Mater. Manuf. Processes **24**, 250 (2009).

[8] P. Siepmann, C. P. Martin, I. Vancea, P. Moriarty, and N. Krasnogor, Nano Lett. **7**, 1985 (2007).

[9] L. Gross, F. Mohn, N. Moll, P. Liljeroth, and G. Meyer, Science **325**, 1110 (2009).

[10] J. A. Stroscio and R. J. Celotta, Science **306**, 242 (2004).

[11] M. Ternes, C. P. Lutz, C. F. Hirjibehedin, F. J. Giessibl, and A. J. Heinrich, Science **319**, 1066 (2008).

[12] Y. Sugimoto, P. Pou, M. Abe, P. Jelinek, R. Perez, S. Morita, and O. Custance, Nature (London) **446**, 64 (2007).

[13] E. Cisternas, F. Stavale, M. Flores, C. A. Achete, and P. Vargas, Phys. Rev. B **79**, 205431 (2009).

[14] G. Terrazas, P. Siepmann, G. Kendall, and N. Krasnogor, J. Cell. Auto. **2**, 77 (2007).

[15] E. Alba and B. Dorronsoro, *Cellular Genetic Algorithms* (Springer, New York, 2008).

[16] N. Q. Huy, Y. S. Ong, M. H. Lim, and N. Krasnogor, Evol. Comput. **17**, 231 (2009).

[17] See supplementary material at http://dx.doi.org/10.1063/1.3600662 for more details on the cellular genetic algorithm approach we have used.

[18] M. Sipper, *Evolution of Parallel Cellular Machines: The Cellular Programming Approach* (Springer, Berlin, 1997).

[19] F. Maes, A. Collignon, D. Vandermeulen, G. Marchal, and P. Suetens, IEEE Trans. Med. Imaging **16**, 187 (1997).

[20] B. J. Albers, T. C. Schwendemann, M. Z. Baykara, N. Pilet, M. Liebmann, E. I. Altman, and U. D. Schwarz, Nat. Nanotechnol. **4**, 307 (2009).